

## Original article

# Design and evaluation of *in-situ* temperature-preserved deep rock coring systems based on analytic hierarchy process

Ling Chen<sup>1,2</sup>, Botao Qin<sup>1</sup>, Yanyan Li<sup>1</sup><sup>\*</sup>, Xun Yang<sup>1</sup>

<sup>1</sup>School of Mechanical Engineering, Sichuan University, Chengdu 610065, P. R. China

<sup>2</sup>State Key Laboratory of Intelligent Construction and Healthy Operation and Maintenance of Deep Underground Engineering, Sichuan University, Chengdu 610065, P. R. China

### Keywords:

Deep rock coring  
heat transfer  
analytic hierarchy process  
optimization  
temperature preservation

### Cited as:

Chen, L., Qin, B., Li, Y., Yang, X. Design and evaluation of *in-situ* temperature-preserved deep rock coring systems based on analytic hierarchy process. *Advances in Geo-Energy Research*, 2025, 16(1): 8-20.  
<https://doi.org/10.46690/ager.2025.04.03>

### Abstract:

The *in-situ* temperature preservation coring of deep rocks is crucial for studying the physical properties of cores under temperature and pressure sensitivity and for assessing resource reserves. Existing core sampling strategies in this field rarely consider temperature preservation, with most employing passive insulation structures based on vacuum technology. In this context, the main challenge is that current insulation technologies and methods cannot meet the requirements of extreme deep environments, necessitating innovative designs of deep *in-situ* insulation coring systems. The insulation system proposed in this paper integrates three subsystems, active insulation, passive insulation, and control system. The analytic hierarchy process is used to perform parametric analysis on the design of these subsystems. By combining heat transfer theory analysis with laboratory pre-research experiments, the evaluation index parameters in the analytic hierarchy process method are quantitatively assigned. This approach further integrates the experience and knowledge of engineering designers to obtain a comprehensive evaluation table of the design parameters. On the basis of the permutation and combination mathematical method, a full matrix set of all feasible conceptual design schemes is established, or the optimal solution is sought through scheme integration, coupling, decoupling, and optimization. The analytic hierarchy process analysis method, which combines theory and pre-experiments, provides a set of parametric analysis methods for conceptual design schemes of insulation coring systems. Furthermore, the optimization of conceptual design schemes through full matrix scheme combinations offers guidance for future data-driven optimization of multi-subsystem conceptual schemes.

## 1. Introduction

With the exploitation of the Earth's mineral resources into deep underground, several challenges have emerged, including high geostress, elevated temperatures, high osmotic pressure, and significant engineering disturbances. Controlling these factors is pivotal for the safe and efficient extraction of subterranean resources (Gao et al., 2018). Temperature plays a critical role in the assessment of deep hydrocarbon reserves and the extraction of coal resources (Sirdesai et al., 2018;

Saif et al., 2019; Mahanta et al., 2020). Traditional coring techniques frequently overlook temperature preservation, leading to inaccurate evaluations of deep oil and gas resources (Sakurovs et al., 2008; Ruckdeschel et al., 2017). As extraction activities gradually intensify, it is becoming increasingly important to consider the impact of temperature on the engineering challenges associated with deep resource extraction. Extreme underground conditions generate multiple technical obstacles: high temperatures and pressures compromise operational stability; mechanical disturbances interrupting data

collection; and spatial constraints limiting technological interventions. Under these circumstances, precise bottom-hole control becomes extremely difficult (Alali et al., 2021; Kazuya and Yosuke, 2021). At the same time, achieving temperature fidelity in core retrieval operations is particularly challenging. To date, only a limited number of pertinent studies and applications have been performed globally in the realm of combustible ice coring and low-temperature preservation. Examples include the Pressure Temperature Core Sampler designed by the Japan Petroleum Corporation (Inada and Koji, 2015), the Multiple Autoclave Corer and Dynamic Autoclave Piston Corer employed in the R.V. SONNE cruise and developed by the Omega Project in Germany, and various high-voltage core retrievers. In China, several devices have been developed for *in-situ* temperature or pressure preservation, including the Pressure and Temperature Preservation System by the Sichuan Institute of Special Sea Technology (Abegg et al., 2008), the bottom-hole frozen core retriever by Jilin University, the TKP-1 thermal insulation and pressure maintenance sampler by the Beijing Institute of Prospecting Engineering, the rope-fishing fidelity sampling drilling tool by the Institute of Exploration Technology, Chinese Academy of Geological Sciences, and the gravity piston fidelity sampler by Zhejiang University (Zhu et al., 2013; Abid et al., 2015). Furthermore, a novel *in-situ* pressure-preserved coring apparatus was developed by Sichuan University (Guo et al., 2024); the Hunan University of Science and Technology established an innovative pressure coring technique specifically tailored for seabed drilling (Wang et al., 2023); and Jilin University presented a newly designed pressure-containing system aimed at enhancing the reliability of pressure retention (Li et al., 2024).

The contemporary coring technologies primarily employ passive thermal insulation strategies based on two main mechanisms: interlayer vacuum techniques and insulating material filling in double-pipe configurations. In addition, surface coating provides supplementary thermal protection. Since there is almost little heat transfer medium after the interlayer has been vacuumed, this significantly reduces the heat conduction rate, thereby achieving efficient insulation effects. However, the current design of seabed sediment insulation corer has a maximum operating depth of 3,000 meters, corresponding to a hydrostatic pressure of 30 MPa. With the design of a sufficiently thick wall, the use of interlayer insulation could meet the requirements under deep-sea pressure. In ultra-deep wells (> 6,000 m) and narrow borehole environments, the persistent application of vacuum interlayer insulation techniques necessitates substantial corer dimensional increases. The vacuum interlayer insulation method would significantly escalate drilling costs and operational complexity. Therefore, the key to insulation coring lies in breaking through the wall thickness limitation without the loss of strength, to achieve a coring system with low thermal conductivity and energy consumption.

One core sampler stands out that employs active thermal insulation: The Japanese Pressure Temperature Core Sampler. Its insulation structure, connected to the core tube via a cable, utilizes a battery-powered Peltier refrigeration unit to maintain low temperatures during subsurface operations. To

supplement this feature, a low-temperature drilling fluid is employed to dissipate heat from the hot end of the Peltier patch, thereby enhancing its cooling efficiency. Additionally, passive thermal insulation measures incorporating insulating materials and liquid nitrogen are also implemented.

In contrast to the aforementioned fidelity core remover, the majority of fidelity core removers developed so far lack effective heat preservation capabilities, particularly in the realm of active thermal insulation. While existing coring equipment is tailored for gas hydrate applications with a focus on low-temperature maintenance, deep terrestrial rock formations often occur at elevated temperatures. In these scenarios, the objective of thermal insulation and coring technology is to prevent core temperature reduction, which is contrary to the low temperature preservation required for seabed sediments. Consequently, the current thermal insulation technologies are not directly applicable to deep-seated thermal insulation and coring.

Considering the aforementioned technical challenges and limitations associated with thermal insulation and coring in terrestrial hard rock, this study delves into the mechanisms and technical requirements for *in-situ* thermal insulation and coring in deep rock formations. Building upon Xie's core device structure (Xie et al., 2024), which facilitates pressure-preserved coring, this research proposes novel technical solutions that integrate active and passive thermal insulation. Furthermore, preliminary indoor experiments and program refinements are conducted to assess the feasibility of these thermal insulation schemes. Fuzzy Analytic Hierarchy Process (AHP) is utilized for a comprehensive evaluation of each approach, which yields the most suitable active and passive thermal insulation plans for deep *in-situ* engineering applications. This study provides essential technical support and design concepts for the development of *in-situ* insulation core technology and equipment tailored for deep rock applications.

## 2. AHP-based design strategy

### 2.1 AHP-based approach for full-cycle product design

The AHP is a multi-criteria decision-making approach extensively applied in manufacturing systems, product design and sustainability assessments (Mardani et al., 2015). Within design applications, AHP is instrumental in prioritizing various product performance indicators (Ishizaka and Labib, 2011). Traditionally, AHP has been employed in the final stages of the design process for evaluating the optimal integrated design solution. However, a limited number of scholars have applied this method to optimize all aspects of the design process.

Considering the sequential nature of deep *in-situ* insulation systems, this study applies AHP throughout the entire product design lifecycle (Mutambo et al., 2022) and proposes an AHP-based full-cycle design strategy, which encompasses the entire process from theoretical foundations to practical application and evaluation. This design strategy is bifurcated into subprogram design and program integration (Dong et al., 2023; Swanepoel et al., 2023), and provides data-driven scientific evaluation and guidance for product design. This

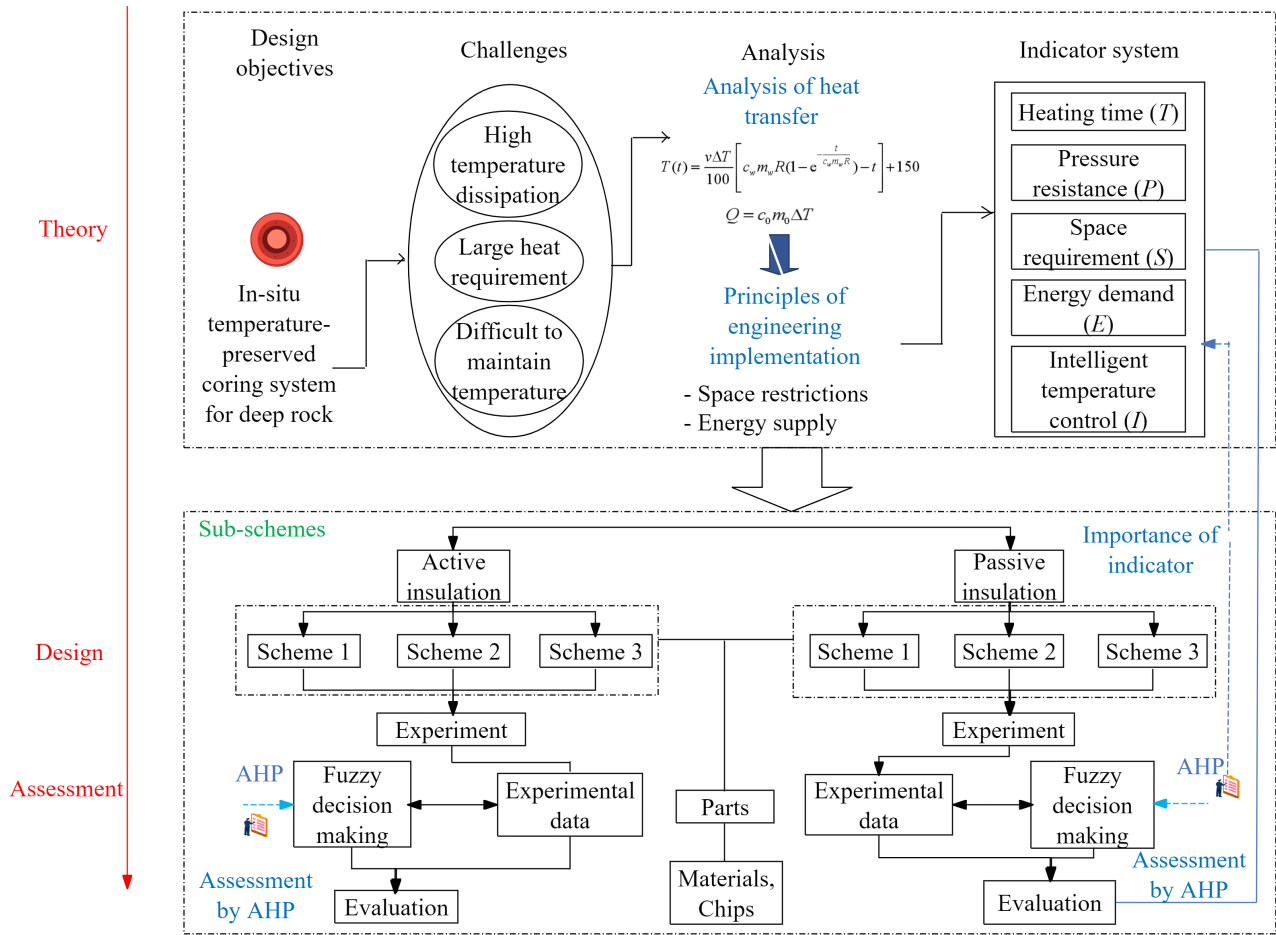


**Fig. 1.** Subprogram design of the insulation system.

approach facilitates efficient, perceptive, scenario-driven, and personalized design solutions (Gocer and Sener, 2022).

The proposed subprogram design is shown in Fig. 1. In the process of deep *in-situ* insulation coring, three problems can be identified: temperature dissipation, heat disturbance and temperature maintenance. For the deep *in-situ* insulation system, the design of subprograms is divided into active thermal insulation and passive thermal insulation. From the principles of the two design directions, a collection of corresponding solutions can be generated. Then, pre-research experiments are carried out for each subprogram and the experimental data are analyzed to determine the parameters of each scheme system. Finally, the index values of each scheme are determined based on the technical parameters, fuzzy decisions and precise experimental data. The AHP method is used to obtain the index weights and finally realize the comprehensive evaluation of the subprograms.

The program integration process is shown in Fig. 2. The subsolution collections generated in the subprogram design phase are classified into three subsystems: unique elements, independent elements, and intersecting elements. The three subsystems are integrated using the principle of permutation and combination to obtain several integrated system solutions. To determine a comprehensive evaluation system for the

integrated system, the design requirements are analyzed and combined with the principles of engineering implementation. Fuzzy decision-making and variable-weight AHP evaluation methods are used to calculate the evaluation values of various integrated solutions with different index weights. According to the application and evaluation results of the previous stage, the solutions are prioritized.

## 2.2 Analysis of heat transfer

In the absence of any thermal insulation measures, the core heat loss from core acquisition to the completion of core lifting is mainly due to the heat conduction caused by changes in the temperature gradient of the formation and the heat conduction caused by heat convection. The shape of the core is a long cylinder and its dimensions are a length of 1,000 mm and a diameter of 50 mm. First, the temperature control and heat transfer model of the core lifting process is established, ignoring the difference in temperature changes at the end of the core. The simplified core thermal model is an infinitely long cylinder, as shown in Fig. 3. From inside to outside, the components are core, core pipe and integrated insulation layer. Among the parameters,  $l$  denotes the length of the core tube heat transfer model, mm;  $R_1$  denotes the core radius and the inner diameter of the core tube, mm;  $R_2$  denotes

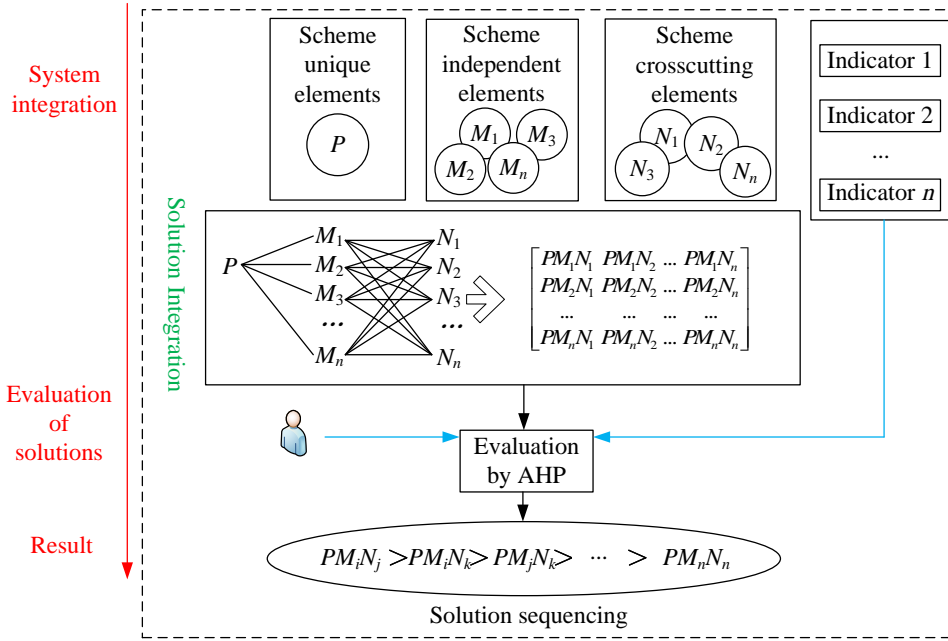


Fig. 2. Process of program integration.

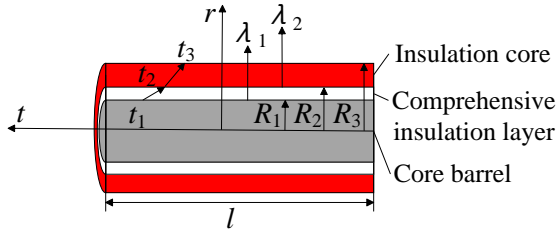


Fig. 3. Simplified core heat-transfer model structure.

the outer diameter of the coring cylinder and the inner diameter of the integrated insulation layer, mm;  $R_3$  denotes the outer diameter of the integrated insulation layer, mm;  $t_1$  denotes the temperature at the contact point between the core and the inner wall of the core tube, K;  $t_2$  denotes the temperature at the contact point between the outer wall of the core tube and the inner wall of the integrated insulation layer, K;  $t_3$  denotes the temperature of the outer wall of the integrated insulation layer, K;  $\lambda_1$  denotes the thermal conductivity of the core tube, W/m·K; and  $\lambda_2$  denotes the thermal conductivity of the integrated insulation layer, W/m·K.

In Fig. 3, the active temperature control system of the coring device is depicted as a three-layer structure comprising a thermal insulation core, coring tube, and comprehensive thermal insulation layer, classifying it as a multilayer cylindrical wall model. Using the principle of superposition of series thermal resistance, the heat conduction heat flow through the multilayer cylindrical wall is expressed by:

$$\phi = \frac{2\pi l(t_1 - t_3)}{\frac{1}{\lambda_1} \ln \frac{R_2}{R_1} + \frac{1}{\lambda_2} \ln \frac{R_3}{R_2}} \quad (1)$$

where the elements are shown in Fig. 3.

According to the definition of thermal resistance and the

principle of superposition of series thermal resistance, the thermal resistance of the multilayer cylindrical wall can be calculated by:

$$R = \frac{\ln \frac{R_2}{R_1} \lambda_2 + \ln \frac{R_3}{R_2} \lambda_1}{2\pi l \lambda_1 \lambda_2} \quad (2)$$

Since the core is at a constant temperature during the coring process and the internal temperature of the core can be considered uniform, the lumped parameter method can be used. Assuming that the initial temperature of the core in the coring tube is  $T(t)$ , as the outside temperature of the core changes during the lifting process, some heat is lost. According to the law of the conservation of energy, Eq. (3) can be obtained by:

$$m_w c_w [T_0 - T(t)] = \int \frac{T(t) - T_a}{R} dt \quad (3)$$

where  $m_w$  denotes the mass of the core, kg;  $c_w$  denotes the specific heat capacity of the core, J/kg·°C;  $T(t)$  and  $T_0$  are respectively the temperature of the core at any time and the initial temperature of the core, °C;  $T_a$  denotes the initial ambient temperature, and  $R$  is the total thermal resistance, °C/W.

The initial core temperature is considered to be consistent with the ambient temperature when obtaining the core *in-situ*. Assuming that the lifting speed of the rope coring is  $v$  (1.67 or 2.5 m/s), the temperature gradient is increased by  $\Delta T$  per 100 meters of depth. While considering the external environmental temperature, the internal core temperature change at any time can be calculated by:

$$T(t) = \frac{v\Delta T}{100} \left[ c_w m_w R \left( 1 - e^{-\frac{t}{c_w m_w R}} \right) - t \right] + 150 \quad (4)$$

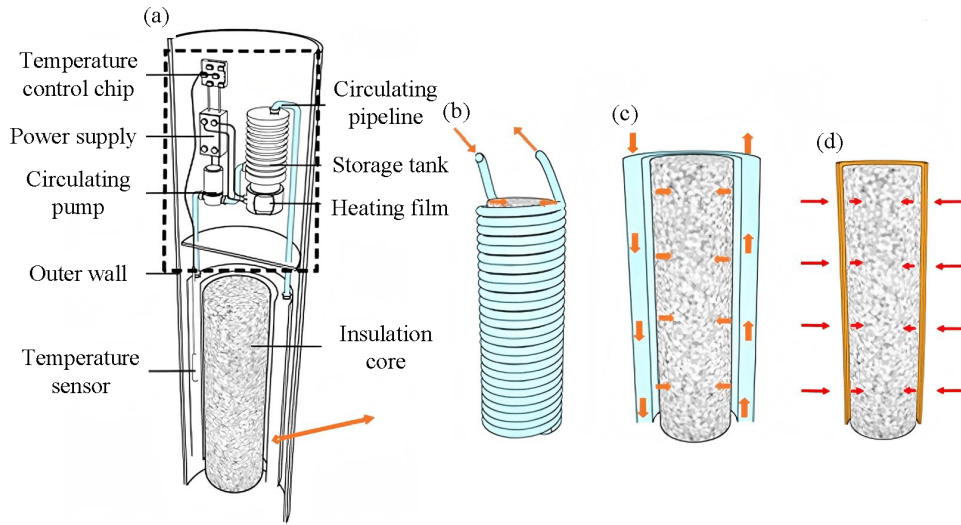


**Fig. 4.** Schematic diagram of the conceptual design of the active thermal insulation scheme. (a) Structure diagram of the coring system, (b) heating film & coil heating, (c) heating & water bath heating and (d) graphene heating.

where  $\Delta T$  is the temperature difference between the environment and the core,  $^{\circ}\text{C}$ .

The average power calculation of the temperature-increasing process is shown by:

$$Q = cm\Delta T(t) = Pt \quad (5)$$

where  $m$  represents the core weight, kg;  $c$  is the core specific heat capacity,  $\text{W/m}\cdot\text{K}$ ;  $T(t)$  is the internal core temperature,  $^{\circ}\text{C}$ .

Assuming that there is only a tiny amount of water formation in the core compartment, most of which is rock-solid, the average specific heat capacity can be set as  $c_0 = 2,000 \text{ J}/(\text{kg}\cdot^{\circ}\text{C})$ . The average density is  $\rho_0 = 2.8 \text{ g}/\text{cm}^3$ . The length of the core chamber is 1,000 mm and the diameter is 50 mm. The energy dissipated can be calculated by:

$$Q_0 = c_0 m_0 \Delta T \quad (6)$$

where  $m_0$  is the weight of the core inside the core chamber.

Therefore, if the heat loss of the core at the bottom of the hole needs to be supplemented during the lifting process, it is required to supplement  $Q_0 = 76,642.12 \text{ J}$  of heat during the lifting process. However, it is challenging to realize the supplementation of this level of heat energy over a long distance in a small deep space. When addressing this issue, it is not only necessary to fully consider the heat compensation of the core under the premise of maximum energy savings, that is, the active and passive integrated insulation schemes of passive thermal insulation and active heating, but also to evaluate and optimize the pros and cons of the schemes under different coring requirements and select the insulation scheme with the best comprehensive performance.

### 3. Experimental setup

In this study, active and passive thermal insulation schemes were designed for deep *in-situ* insulation coring, then indoor pre-research experiments were conducted. The selected criteria

for optimization scoring included heating time ( $T$ ), pressure-resistant properties ( $P$ ), space requirement ( $S$ ), energy consumption demand ( $E$ ), and intelligent temperature control ( $I$ ) for each scheme. The active thermal insulation schemes consisted of heating films paired with a water bath, heating films with coils, and those with graphene, while the passive thermal insulation schemes included vacuum insulation structures, polyurethane foam, aerogel, and vacuum glass microspheres.

#### 3.1 Active thermal insulation

The active thermal insulation system considers the narrow-space working conditions and heating uniformity during deep *in-situ* actual operation. To make full use of its axial space, an active thermal insulation system using a liquid medium as the heat transfer carrier in the axial space was designed inside the core remover. The schemes include a direct water bath heating scheme using a heating film as the heating source, a diversion heat transfer scheme that increases the heat transfer area through the coil, and direct heating of the core using a graphene heater as the heating source (Chung et al., 2020; Ilmola et al., 2021). The conceptual design of the three schemes is shown in Fig. 4.

The structure and principle diagram of the *in-situ* active insulation system for deep rock formations mainly includes a temperature control chip, low-voltage direct current power supply, circulating water pump, circulating pipeline, water storage tank, heating film, temperature sensor, and heat-carrying fluid medium. The active insulation chip is in an enclosed structure, hence it does not operate directly in a high water-pressure environment. Therefore, the active insulation chip only needs to meet the high temperature tolerance requirement ( $150^{\circ}\text{C}$ ). The heating film and heating circuit in the active insulation only work in high-pressure environments without differential pressure; thus, the active insulation does not need to have high compressive strength.

According to the conceptual design plan, the experimental research design was carried out. Therein, a heating film is

used as a heating source to heat the circulating heat carrier medium, and the heat is transferred to the constant-temperature test container in a direct water bath and a coil. To heat the target directly, a graphene heater is used as the heat source. The core temperature is actively controlled by two methods: the direct water bath and the spiral coil. To actively control the core's temperature without needing a heating medium and circulation pipelines, the graphene heater is used as a direct heating method. The heating film used in the experiment is insulated and has a thickness of 10 mm. For the coil, an inner diameter of 2 mm was chosen to optimize flow performance. The graphene heater is a thin-walled cylinder with a wall thickness of 1 mm.

### 3.2 High temperature resistance test

The desired target temperature is set using a temperature control chip and is compared to the value measured by the temperature sensor in the constant-temperature test chamber. The temperature control chip outputs a control signal to adjust the heating film's working state accordingly. The regulation and maintenance of the target temperature is realized by the heat energy of the carrier fluid.

The temperature sensor and control switch (metal oxide semiconductor tube) are integrated into a temperature control chip. The active temperature control chip is made of high-temperature resistant components, all of which have passed the AEC-Q100 (grade 0) certification and can typically work in the temperature range of -40-150 °C. To verify the high-temperature resistance of the control chip in widespread use, a certain amount of heat transfer oil is placed into the beaker container as the heat preservation object. A graphene sheet is installed in the container as an active thermal insulation material, and a 12 V power supply is used to form a loop with the chip. Moreover, a low-voltage power supply (6.8 V/0.03 A) is provided separately for the chip to ensure its smooth function. The chip is placed in an oven, where a temperature sensor records and displays the thermal oil temperature in real-time.

Since the temperature control chip is placed inside the central rod during operation, there is no need to consider the impact of high pressure. Herein, only the temperature resistance test is performed. During the experiment, the oven temperature was set to be stable at 80, 100, 120, 140 and 160 °C to simulate the *in-situ* environmental temperature of different temperature gradients and test the operational stability of the chip in different *in-situ* temperature environments.

### 3.3 Passive thermal insulation

Passive thermal insulation has been used extensively in practical engineering applications. This paper explores the specific conditions and requirements for *in-situ* coring, integrating traditional passive thermal insulation materials and structures with innovations for small spaces, high-pressure environments, and strength requirements (He et al., 2020). Then, it focuses on minimizing any disturbances to core temperature while meeting the spatial constraints. Given that core removers are typically located deep underground and must withstand the

significant disturbances caused by drilling processes, a comparative analysis of insulation materials—including hollow glass microspheres (HGM), vacuum structures, polyurethane foam, and aerogels—was conducted, with a focus on thermal conductivity. Furthermore, a comparative analysis was performed on the strength requirements of aerogel and hollow glass microsphere materials (Li et al., 2011, 2020; Bi et al., 2014).

In order to evaluate the thermal insulation performance of four passive thermal insulation methods, heat transfer oil was used as the heating medium, which was placed in test containers, each employing a different insulation method. The containers were then placed in an oven, which was gradually heated from room temperature to 150 °C. After the oil temperature stabilized, the oven was turned off and the test samples were allowed to cool to room temperature. The temperature and time values during the whole process of the four curves were recorded.

Regarding the strength and thermal insulation performance requirements, the optimization of vacuum structures and polyurethane insulation materials was not considered. To further assess the differences in performance between aerogel and hollow glass microspheres, a thermal insulation energy consumption test was conducted. To highlight the energy-saving performance of thermal insulation materials, the Peltier cooler and heating film composite heat transfer method was used for temperature control.

## 4. Experimental results and discussion

### 4.1 Temperature preservation

On the basis of the structure and schematic diagram of the active thermal insulation system, an indoor experimental platform was constructed. The medium in the constant temperature test container was actively controlled by various heat transfer mechanisms. The constant heating temperature was maintained at 80 °C. The experimental results are shown in Fig. 5.

From the temperature-time curves of the different experimental schemes in the above figure, it can be seen that the three heat transfer methods have significant differences considering to the total heating time, average heating rate and maximum heating rate in terms of the heat transfer at different stages. In addition, the changes in the voltage values during the heating process were measured in the experiment using a shunt, as shown in Fig. 6.

In the experiment, the shunt specifications were  $U_0 = 75$  mV and  $I_0 = 20$  mA. From the voltage-time curves, it can be seen that the voltage of the shunt connected to the graphene and to the heating film is  $U_1 = 36.4$  mV and  $U_2 = 16$  mV, respectively. A multimeter measures the voltage at both ends of the graphene heater when it is working ( $U_3 = 11.16$  V) and when the heating film is working ( $U_4 = 11.64$  V). When the water temperature rises to the set temperature of 80 °C, the energy consumed by the two heating methods can be calculated by:

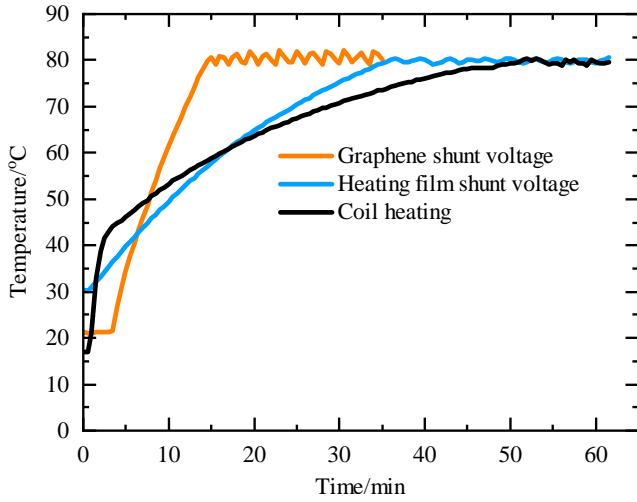


**Fig. 5.** Temperature control results for different heat transfer forms.

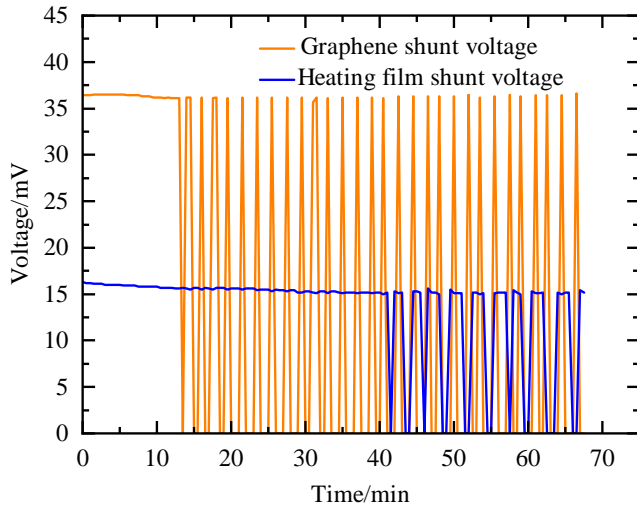


**Fig. 6.** Changes in voltage during the heating process.

**Table 1.** Performance indicators of different heat transfer methods.

Evaluation criteria	Graphene heater	Coil heating	Heating film
$T$	12	34	44
$v_T$	6.67	2.35	1.82
$T_{\max}$	5.1	1.39	10.36
$d/D$	1.5/51	6/51	3/51
$E_{rr}$	2.75	0.75	0.00125

$$W_3 = U_3 \frac{U_1 I_0}{U_0} T_3 \quad (7)$$

$$W_4 = U_4 \frac{U_2 I_0}{U_0} T_4 \quad (8)$$

where  $T_3$  represents the heating time of the graphene heating scheme, °C; while  $T_4$  is the heating time of the heating film

scheme, °C. In contrast, under the exact heating requirements, the former graphene heater saves 39,236.364 J of energy from the energy consumption perspective compared to the heating membranes.

In this study, the different heating indicators are sorted out, as shown in Table 1, where  $T$  denotes heating time, min;  $v_T$  denotes average heating rate, °C/min;  $T_{\max}$  represents maximum heating rate;  $d/D$  denotes heater wall thickness/core diameter;  $E_{rr}$  is temperature control accuracy, %.

As seen from the above data, the excellent heating performance of graphene combined with direct heating has obvious advantages in terms of both heating time and heating rate. In the early stage, due to the significant temperature difference and large heat transfer area, the coil heating method results in the phenomenon of rapid heat transfer and warming in a short period. However, as the temperature difference decreases, the comprehensive heating efficiency of the coil heating method remains inferior to that of the indirect water bath heating method. The thermal insulation model of water bath heating requires the addition of thermal convection and thermal radiation, yet the corresponding heating efficiency and heating time are better than those of graphene and coils. Besides, the wall thickness of the water bath joiner is much greater than those of the other two heating methods, which is unsuitable for the insulation requirements of small spaces. In terms of heat transfer efficiency and heating power, graphene is superior to the other two heating methods. The heating film is superior to the coil-based heat transfer when the target temperature is higher than 60 °C. The graphene heater is incorporated into the optimal program when selecting the active temperature control program, considering the heating time, energy consumption, space size, etc.

Taking the design analysis by AHP as a basis, a simulation system for experimental testing of active and passive thermal insulation has been constructed, as illustrated in Fig. 7.

In order to evaluate the thermal insulation capabilities and error margins of the insulation system, this system simulates various *in-situ* deep geothermal environments, with the test results shown in Fig. 8. The maximum temperature fluctuations of the different constant temperatures are 1.28%, 1.07%, 0.55%, 0.24%, and 0.2%, which are proportional to the corresponding constant temperature values. Moreover, the chip's temperature resistance can reach 160 °C, which meets the temperature resistance limit requirements.

The temperature-time curve in Fig. 9, measured during the experiment shows that the vacuum structure has a faster heating rate than the other two passive thermal insulation methods and a weaker insulation effect. In comparison, the cooling rate is slower than that of the other three methods. The vacuum degree is considered reduced and the heat transfer area of the vacuum structure is low. Aerogels, hollow glass microspheres and polyurethane exhibit little differences in thermal insulation performance. However, because polyurethane is a foam material, its structure contains many pores, resulting in a low overall mechanical strength, which does not meet the requirements of practical applications.

As described in Table 2,  $\lambda$  represents thermal conductivity, W/mK;  $v_{\max}$  represents maximum cooling rate, K/s;  $d/D$  is

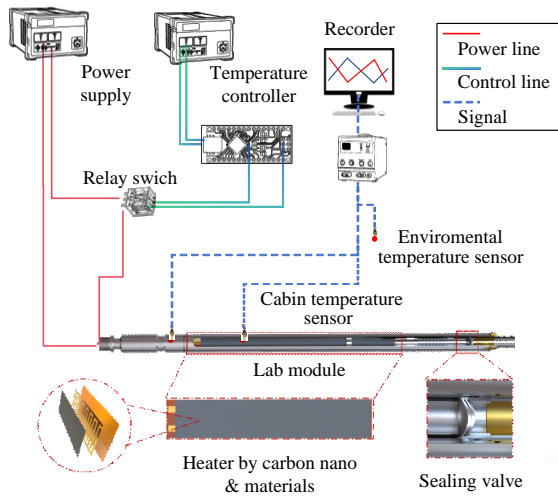


**Fig. 7.** Simulation system for active and passive thermal insulation experimental testing.

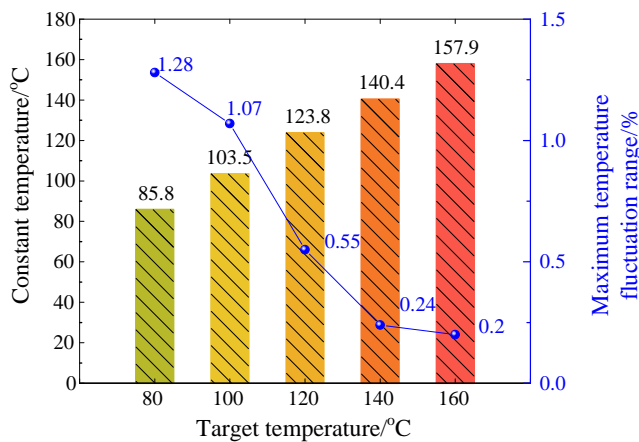


**Fig. 8.** Result of the chip-controlled insulation experiment and the maximum temperature fluctuation range.

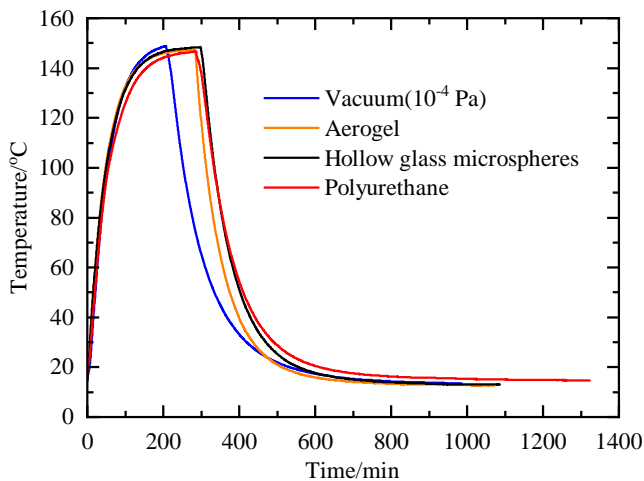


**Fig. 9.** Thermal insulation results of different passive thermal insulation forms.

equal to thickness/core diameter. Among the four passive thermal insulation materials, hollow glass microspheres have

**Table 2.** Technical parameters of the four passive thermal insulation methods.

Indicators	HGM	Polyurethane	Aerogel	Vacuum
$\lambda$	0.033	0.022	0.013	0.023
$v_{\max}$	0.833	0.917	1.041	1.125
$d/D$	2	2.5	2	2.5
Anti-corrosion	Excellent	Varies	Good	Excellent
Thermal stable	Excellent	Good	Excellent	Varies

**Table 3.** Properties of passive insulation materials.

Index	Aerogel	Polyurethane	Vacuum	HGM
$\lambda$	0.023	0.029	0	0.137
$\sigma$	3.7	0.28	0	51.2

the most significant thermal conductivity. This is because aerogel and vacuum materials introduce thermal convection and thermal radiation, respectively, resulting in more heat dissipation, so the maximum cooling rates of both the aerogel and vacuum materials are more significant than that of the hollow glass microspheres.

Polyurethane, albeit having a smaller thermal conductivity than hollow glass microspheres, results in a more significant cooling rate due to its poorer corrosion resistance and the unstable nature of the insulation. The thermal conductivity and compressive strength properties of the four materials are shown in Table 3, where  $\lambda$  represents thermal conductivity, W/mK; and  $\sigma$  is compressive strength, MPa.

Firstly, the thermal conductivity of aerogel and polyurethane foam is low, along with the compressive strength. In the high water pressure characterizing the deep *in-situ* environment, their structures and insulation ability will be lost. Secondly, the thermal conductivity of the vacuum layer is low, but the reinforcement layer still needs to be added to the core, increasing the core's size, and thus significantly increasing the cost of the deep coring. In addition, the size of the corer required for the vacuum layer exceeds the size limit of the *in-situ* temperature-preserved coring device. Hollow glass microspheres are the preferred choice for corrosive resistance, insulation stability, and a lower cooling rate.

#### 4.2 Program evaluation

AHP was used to obtain the weights of each indicator and to combine the theoretical model, experimental data and fuzzy expert decisions. From the theoretical model and the research experimental data, a table of parameters could be obtained and used as the basis for evaluation. The affiliation of the qualitative and quantitative indicators to specific levels was obtained using the expert evaluation method and the affiliation function, respectively.

According to pre-researched experimental settings and actual coring requirements, the mapping relationship between experimental data and functional requirements was established, the relationship between each experimental parameter and the indicator layer was determined, and the evaluation level of the indicator layer was set.

In the program evaluation, the criteria membership set  $\mathbf{B} = \{\text{excellent, good, inferior}\}$ , and 0.9, 0.6, 0.3 were used to represent the satisfaction degree scores of the three indicators of excellent, good and poor, respectively. The program indicators were divided into qualitative and quantitative indicators, and their rank affiliations corresponding to rank set  $\mathbf{B}$  were obtained separately using different methods.

Qualitative indicators, based on the parameter table, were obtained by the expert evaluation method. If there are  $H$  experts scoring them, the  $k_{ih}$  expert's evaluation result for a particular indicator  $i$  is  $(u_{i1}^k, u_{i2}^k, u_{i3}^k)$  where  $(u_{i1}^k, u_{i2}^k, u_{i3}^k)$  takes the value of 0 or 1, representing the experts' votes for the evaluation set of (excellent, good and poor), and the affiliation of indicator  $i$  to the evaluation set (excellent, good and poor) can be calculated by Eq. (9), respectively:

$$r_{i1} = \frac{\sum_{k=1}^H u_{i1}^k}{\sum_{k=1}^H \sum_{j=1}^3 u_{ij}^k}, r_{i2} = \frac{\sum_{k=1}^H u_{i2}^k}{\sum_{k=1}^H \sum_{j=1}^3 u_{ij}^k}, r_{i3} = \frac{\sum_{k=1}^H u_{i3}^k}{\sum_{k=1}^H \sum_{j=1}^3 u_{ij}^k} \quad (9)$$

where  $r_{i1}$ ,  $r_{i2}$ ,  $r_{i3}$  are the affiliations of indicator  $i$ . For quantitative indicators, an affiliation function was obtained using the pre-researched experimental data as well as a table of parameters. Based on the characteristics of the corer indicators and the evaluation level  $\mathbf{S} = \{\text{excellent, good, poor}\}$ , a combined trapezoidal and triangular affiliation function was used.

The corresponding formulas are expressed by:

$$r_{i1} = \begin{cases} 1 & 0 < x < x_1 \\ \frac{x_2 - x}{x_2 - x_1} & x_1 < x < x_2 \\ 0 & x > x_2 \end{cases} \quad (10)$$

$$r_{i2} = \begin{cases} \frac{x - x_1}{x_2 - x_1} & x_1 < x < x_2 \\ \frac{x_3 - x}{x_3 - x_2} & x_2 < x < x_3 \\ 0 & x > x_3 \text{ or } x < x_1 \end{cases} \quad (11)$$

$$r_{i3} = \begin{cases} 1 & x_3 < x < x_4 \\ \frac{x - x_2}{x_3 - x_2} & x_2 < x < x_3 \\ 0 & x < x_2 \end{cases} \quad (12)$$

To discuss the corresponding scoring results and sensitivity differences under different importance scales, this paper takes graphene heating in active thermal insulation as an example. Based on the functional importance of the deep rock temperature-preserved coring system, the target evaluation was first established and the relative importance of each index was evaluated by AHP. The judgment matrix was established with

$T$ ,  $S$ ,  $P$ ,  $E$ , and  $I$  as those with the highest level of importance. When the heating time is more important than other criteria, the corresponding importance descriptions of the other criteria are as shown in Table 4, where  $T$  represents heating time,  $S$  represents space requirement,  $P$  denotes pressure-resistant properties,  $E$  denotes energy consumption demand, and  $I$  is intelligent temperature control. From the following table, the fuzzy evaluation matrix and comprehensive evaluation scores of graphene heating can be obtained.

Through the above mentioned fuzzy scale table, each index was analyzed and transformed, and the fuzzy complementary judgment matrix  $\mathbf{A}$  was constructed according to the relative importance relationships. The calculation method of matrix  $\mathbf{A}$  is shown in:

$$\mathbf{A} = \begin{bmatrix} & T & S & P & E & I \\ T & 0.5 & 0.6 & 0.6 & 0.7 & 0.7 \\ S & 0.4 & 0.5 & 0.4 & 0.7 & 0.8 \\ P & 0.4 & 0.6 & 0.5 & 0.7 & 0.8 \\ E & 0.3 & 0.3 & 0.3 & 0.5 & 0.4 \\ I & 0.3 & 0.2 & 0.2 & 0.6 & 0.5 \end{bmatrix} \quad (13)$$

Eqs. (14) and (15) can transform matrix  $\mathbf{A}$  into the fuzzy consistency matrix  $\mathbf{B}$  by:

$$b_i = \sum_{k=1}^l a_{ij} \quad (14)$$

$$b_{ij} = \frac{b_i - b_j}{2n} + 0.5 \quad (15)$$

where  $a_{ij}$  and  $b_{ij}$  correspond to the unit of matrix  $\mathbf{A}$  and  $\mathbf{B}$  respectively, and  $l$  is the evaluation index. The fuzzy consistency matrix  $\mathbf{B}$  can be calculated by:

$$\mathbf{B} = \begin{bmatrix} 0.50 & 0.53 & 0.51 & 0.63 & 0.63 \\ 0.47 & 0.50 & 0.48 & 0.60 & 0.60 \\ 0.49 & 0.52 & 0.50 & 0.62 & 0.62 \\ 0.37 & 0.40 & 0.38 & 0.50 & 0.50 \\ 0.37 & 0.40 & 0.38 & 0.50 & 0.50 \end{bmatrix} \quad (16)$$

On the basis of the fuzzy consistency judgment matrix, the weight is calculated by:

$$w_j = \frac{\sum_{j=1}^i b_{ij} + \frac{n}{2} - 1}{n(n-1)} \quad (17)$$

Then, the subjective weight value vector of each index is shown in:

$$\mathbf{w} = [0.231, 0.218, 0.226, 0.176, 0.176] \quad (18)$$

In Sections 4.1, technical parameter tables for different active and passive thermal insulation systems could be obtained. On this basis, the affiliation values for each indicator corresponding to the evaluation level set were obtained according

**Table 4.** Evaluation grades.

Criteria and weights	Evaluation grade		
$T(0.231)$	0.9	0.1	0
	0.85	0.05	0.1
$S(0.218)$	0.9	0.1	0
	0.9	0.1	0
$P(0.226)$	0.85	0.15	0
	0.75	0.25	0
$E(0.176)$	0	0	0
	0.8	0.2	0
$I(0.176)$	0.75	0.25	0
	0.9	0.1	0

**Table 5.** Ranking of scores under different importance criteria for active thermal insulation schemes.

Schemes	Importance criteria				
	$T$	$S$	$P$	$E$	$I$
Graphene	82.2	82.5	82.9	78	81.1
Film & coil	72.9	71.8	72.8	69	72.2
Film & water bath	72.4	72.9	73.2	68.7	71.9

to the method of calculating the affiliation described in Section 4.3. Graphene heating in active thermal insulation was taken as an example to evaluate its various indices.

The set of evaluation criteria membership degree can be selected by:

$$\mathbf{R}_1 = \begin{bmatrix} 0.8825 & 0.0825 & 0.035 \\ 0.9 & 0.1 & 0 \\ 0.8 & 0.2 & 0 \\ 0.52 & 0.13 & 0 \\ 0.825 & 0.175 & 0 \end{bmatrix} \quad (19)$$

$\mathbf{C} = \{C_1, C_2, C_3\}^T = \{0.9(\text{good}), 0.6(\text{average}), 0.3(\text{poor})\}^T$ . The comprehensive evaluation score can be calculated by:

$$\text{score} = 100wR_1C = 82.168 \quad (20)$$

where  $w$  represents the subjective weight value vector of each index. That is, when the heating time is the most important criterion, the score of the graphene heating is  $S_T = 82.168$ . Moreover, when the criteria of  $S$ ,  $P$ ,  $E$ , and  $I$  are more important than other criteria, the scores of graphene heating schemes can be calculated by:

$$S_s = 82.547, S_p = 82.852, S_E = 77.958, S_I = 81.145 \quad (21)$$

In the same fashion, the scores of 'heating film and water bath' and 'heating film and coil' and passive thermal insulation solutions corresponding to different importance criteria were obtained. The different importance criteria of all solutions were then classified and arranged.

From the above two tables, it can be inferred that when scoring active thermal insulation schemes in terms of different essential criteria, the optimal scheme involves graphene heating materials that have low sensitivities and high stabilities and are the best choice of insulating material for the active thermal insulation scheme. For the passive thermal insulation scheme, hollow glass microsphere composites are the best choice of insulating material when  $S$  and  $P$  are the most important criteria, and the vacuum material is the best choice of material when 'energy consumption' is the most important criterion. However, hollow glass microsphere composites are still the best choice of material with the lowest sensitivity and relatively higher stability out of all the passive thermal insulation solutions and are the optimal choice of material for the passive thermal insulation scheme.

### 4.3 Solution integration

The previous section followed the two main design directions of active temperature control and passive thermal insulation, yielding sub-solutions including heating film and water bath heating, graphene, vacuum and aerogel insulating materials, and the design of high-temperature chips. From the analysis of the active and passive thermal insulation effects in the previous section, the subsolutions are integrated, resulting in an integrated thermal insulation system that meets the design requirements. First, the subprograms are classified into three main collections of elements: Unique elements, independent elements, and cross elements.

For the combined integrated solution system, the single-layer index system and the fuzzy AHP evaluation method are used to calculate the evaluation value of each integrated solution. The solutions are prioritized, the experimental data are combined, and the analysis results of the subsolutions are obtained to finally achieve the comparative preference of the integrated solutions.

The fuzzy evaluation matrix of the combined solution can be derived from that of the subsolutions. When considering a combination of several technical solutions to achieve product design innovation, it is necessary to obtain the technical combination of solutions to meet a certain degree of compatibility. In this paper, the main passive thermal insulation is technically compatible, but after the combination of each subprogram to the overall solution, the effects of the contribution degree are different. According to the construction of the contribution degree matrix, the fuzzy evaluation matrix of the combination of solutions is obtained.

Therein,  $k_{ij}^a$  indicates subprogram  $M_i$  for the contribution of the combined program  $PM_iN_j$  to the  $a_{th}$  indicator, and likewise for subprogram  $N_j$  for the contribution of the combined program  $PM_iN_j$  to the contribution matrix.  $K'_{N_jM_i}$  can be calculated by:

**Table 6.** Contributions of each active and passive thermal insulation subprogram.

Contribution to matrix	Contribution to indicator			
	$N_1$	$N_2$	$N_3$	$N_4$
$M_1$	diag(1,0.5,0.5,0.5,1)	diag(1,0.5,0.6,0.5,1)	diag(1,0.5,0.5,0.5,1)	diag(1,0.5,0.5,0.4,1)
$M_2$	diag(1,0.5,0.5,0.6,1)	diag(1,0.5,0.6,0.5,1)	diag(1,0.5,0.5,0.4,1)	diag(1,0.5,0.5,0.4,1)
$M_3$	diag(1,0.6,0.5,0.5,1)	diag(1,0.5,0.6,0.5,1)	diag(1,0.5,0.5,0.5,1)	diag(1,0.5,0.5,0.4,1)

$$\mathbf{K}'_{N_j M_i} = \text{diag}(1, 1, 1, 1, 1) - \mathbf{K}_{M_i N_j} \quad (22)$$

If the fuzzy evaluation matrix of the active insulation subprogram  $R_{M_i}$  with the fuzzy evaluation matrix of the passive thermal insulation sub-scheme  $R_{N_j}$ , then the fuzzy evaluation matrix of the combined scheme is shown in:

$$\mathbf{R}_{PM_i N_j} = \mathbf{K}_{M_i N_j} \mathbf{R}_{M_i} + \mathbf{K}'_{N_j M_i} \mathbf{R}_{N_j} \quad (23)$$

A two-dimensional table of the contributions of the combined active and passive thermal insulation subprograms was constructed by analyzing the effects of each subprogram and combination of programs as described below.

Based on the data in Table 6, the evaluation value of the portfolio option  $PM_1 N_1$  can be calculated by:

$$\mathbf{K}_{M_1 N_1} = \text{diag}(1, 0.5, 0.5, 0.5, 1) \quad (24)$$

$$\mathbf{K}'_{N_j M_i} = \text{diag}(1, 0.5, 0.5, 0.5, 1)$$

$$\mathbf{R}_{M_1} = \begin{bmatrix} 0.8825 & 0.0825 & 0.035 \\ 0.9 & 0.1 & 0 \\ 0.8 & 0.2 & 0 \\ 0.52 & 0.13 & 0 \\ 0.825 & 0.175 & 0 \end{bmatrix}, \dots \quad (25)$$

$$\mathbf{R}_{N_1} = \begin{bmatrix} 0 & 0 & 0 \\ 0.4875 & 0.1625 & 0 \\ 0.75 & 0.15 & 0.1 \\ 0.2625 & 0.0875 & 0 \\ 0 & 0 & 0 \end{bmatrix}$$

$$\mathbf{R}_{PM_1 N_1} = \mathbf{K}_{M_1 N_1} \mathbf{R}_{M_1} + \mathbf{K}'_{N_1 M_1} \mathbf{R}_{N_1} = \begin{bmatrix} 0.08825 & 0.07 & 0.035 \\ 0.6938 & 0.1313 & 0 \\ 0.775 & 0.175 & 0.05 \\ 0.3913 & 0.1088 & 0 \\ 0.825 & 0.175 & 0 \end{bmatrix} \quad (26)$$

The set of evaluation criteria membership degrees is selected by:

$$\mathbf{C} = \{C_1, C_2, C_3\}^T = \{0.9(\text{good}), 0.6(\text{average}), 0.3(\text{poor})\}^T \quad (27)$$

The comprehensive evaluation score is shown in:

$$\text{score}(PM_1 N_1) = 100wR_{PM_1 N_1} C = 75.588 \quad (28)$$

where  $w$  represents the subjective weight value vector of each index, shown in Eq. (16). Using the same method, the evaluation scores for each program were calculated by Eq. (29) to form the evaluation value matrix:

$$\mathbf{F} = \begin{bmatrix} 75.588 & 74.607 & 73.674 & 72.707 \\ 70.810 & 69.190 & 68.085 & 67.5789 \\ 69.924 & 68.012 & 67.521 & 66.571 \end{bmatrix} \quad (29)$$

On the basis of the magnitude of the values in the matrix, the matrix  $F$  is transformed into a vector of solution advantages and disadvantages, which is shown in:

$$\mathbf{Y}_T = (PM_1 N_1 \ PM_1 N_2 \ PM_1 N_3 \ PM_1 N_4 \ PM_2 N_1 \ PM_2 N_2 \ PM_2 N_3 \ PM_2 N_4 \ PM_3 N_1 \ PM_3 N_2 \ PM_3 N_3 \ PM_3 N_4) \quad (30)$$

The above is the sequence vector for the scenario when the criterion of time has the maximum weight. Following the same method, when the space requirements, pressure resistance, energy demand, and intelligent temperature control are set as the maximum priorities, the following are calculated by:

$$\mathbf{Y}_S = (PM_1 N_1 \ PM_1 N_2 \ PM_1 N_3 \ PM_1 N_4 \ PM_2 N_1 \ PM_2 N_2 \ PM_2 N_3 \ PM_2 N_4 \ PM_3 N_1 \ PM_3 N_2 \ PM_3 N_3 \ PM_3 N_4) \quad (31)$$

$$\mathbf{Y}_P = (PM_1 N_1 \ PM_1 N_2 \ PM_1 N_3 \ PM_1 N_4 \ PM_2 N_1 \ PM_2 N_2 \ PM_2 N_3 \ PM_2 N_4 \ PM_3 N_1 \ PM_3 N_2 \ PM_3 N_3 \ PM_3 N_4) \quad (32)$$

$$\mathbf{Y}_E = (PM_1 N_1 \ PM_1 N_2 \ PM_1 N_3 \ PM_1 N_4 \ PM_2 N_1 \ PM_2 N_2 \ PM_2 N_3 \ PM_2 N_4 \ PM_3 N_1 \ PM_3 N_2 \ PM_3 N_3 \ PM_3 N_4) \quad (33)$$

$$\mathbf{Y}_I = (PM_1 N_1 \ PM_1 N_2 \ PM_1 N_3 \ PM_1 N_4 \ PM_2 N_1 \ PM_2 N_2 \ PM_2 N_3 \ PM_2 N_4 \ PM_3 N_1 \ PM_3 N_2 \ PM_3 N_3 \ PM_3 N_4) \quad (34)$$

As seen from the priority sequence of the combined scheme, regardless of which index is given priority, scheme  $PM_1 N_1$ , i.e., the combined scheme “chip+graphene heating+vacuum microtubes” achieves the greatest evaluation value and has the best insulation effect, thus is the optimal scheme for deep *in-situ* fidelity coring. A structural design of this scheme is shown below in Fig. 10.

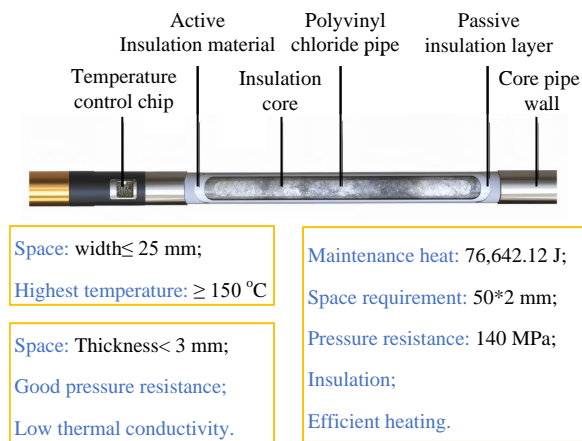


**Fig. 10.** Structural design of the scheme *in-situ* temperature preserved coring system.

For the design-generated deep insulation core optimization scheme, active and passive indoor tests were carried out. Indoor pre-research experiments were conducted under graphene heating conditions as well as under hollow glass microsphere material conditions. The relevant scheme has been verified in the team's simulation experiment. Long-term validation tests have been completed, successfully maintaining core temperatures for 169.3 hours during simulated coring (Xie et al., 2024).

## 5. Conclusions

This study aimed to develop an effective insulation coring system for deep rock applications, focusing on enhancing the accuracy of design parameters and optimizing the system's performance under extreme conditions. Using a combination of theoretical analysis and experimental validation, the research achieved significant progress in designing an insulation system capable of maintaining core sample integrity at high temperatures and pressures. Based on the findings, the main conclusions drawn from this study are as follows:

- 1) A non-steady-state heat transfer model was developed on the basis of the heat transfer theory. This model provides a parametric expression of design requirements for the insulation coring system, laying a solid theoretical foundation for its conceptual design. On this basis, an insulation system was proposed, consisting of an active insulation system, a passive insulation system, and a control system.
- 2) For the active insulation system, the graphene heater solution improves the heat exchange efficiency compared with coil heating and heating film heating, respectively. At the same time, the volume, energy-saving and reliability of the control device are greatly improved. The 0.2% maximum temperature fluctuation range at 160 °C is realized, which verifies the device's feasibility.
- 3) For passive insulation, under the priority to meet the compressive strength, the vacuum microbead composite material saves 6.66 kJ compared with the aerogel composite structure, and with the increase in time and temperature,

its advantages are more prominent. Although the vacuum structure has the best thermal insulation performance, it is not easy to meet the actual engineering application requirements regarding system reliability, strength and size.

- 4) Laboratory pre-experiments results supplied the fundamental data required for the AHP method, enabling accurate evaluation of each sub-scheme. By coupling multiple schemes of the three major subsystems of the insulation system, a mathematical full matrix optimization algorithm was constructed. This algorithm facilitated a comprehensive evaluation and selection of the optimal design scheme via a systematic approach.

The composition of the rock insulation system was specified to include graphene-based active heating and vacuum microsphere passive insulation. This configuration successfully achieved the conceptual design of the insulation system for operation under conditions of 150 °C and 140 MPa.

Looking ahead, while this study has made substantial contributions to the design of insulation coring systems, the practical effectiveness and robustness of the proposed design under real-world conditions have not been validated through field trials. Future research should integrate advanced data-driven techniques and conduct extensive field experiments.

## Acknowledgements

This work was supported by the National Key Research and Development Program of China (No. 2022YFB3706600), the National Natural Science Foundation of China (Nos. 52225403 and 52274133). The authors also thank the editor and anonymous reviewers for their valuable advice.

## Conflict of interest

The authors declare no competing interest.

**Open Access** This article is distributed under the terms and conditions of the Creative Commons Attribution (CC BY-NC-ND) license, which permits unrestricted use, distribution, and reproduction in any medium, provided the original work is properly cited.

## References

- Abegg, F., Hohnberg, H. J., Pape, T., et al. Development and application of pressure-core-sampling systems for the investigation of gas-and gas-hydrate-bearing sediments. *Deep Sea Research Part I: Oceanographic Research Papers*, 2008, 55(11): 1590-1599.
- Abid, K., Spagnoli, G., Teodoriu, C., et al. Review of pressure coring systems for offshore gas hydrates research. *Underwater Technology*, 2015, 33(1): 19-30.
- Alali, A. M., Abughaban, M. F., Aman, B. M., et al. Hybrid data driven drilling and rate of penetration optimization. *Journal of Petroleum Science and Engineering*, 2021, 200: 108075.
- Bi, C., Tang, G., Hu, Z. Heat conduction modeling in 3-d ordered structures for prediction of aerogel thermal conductivity. *International Journal of Heat and Mass Transfer*, 2014, 73: 103-109.
- Chung, Y., Chung, H., Lee, Y., et al. Heat dissipation and

- electrical conduction of an led by using a microfluidic channel with a graphene solution. *Applied Thermal Engineering*, 2020, 175: 115383.
- Cinelli, M., Coles, S. R., Kirwan, K. Analysis of the potentials of multi criteria decision analysis methods to conduct sustainability assessment. *Ecological Indicators*, 2014, 46: 138-148.
- Dong, L., Zhu, H., Yan, F., et al. Risk field of rock instability using microseismic monitoring data in deep mining. *Sensors*, 2023, 23(3): 1300.
- Gao, M., Zhang, R., Xie, J., et al. Field experiments on fracture evolution and correlations between connectivity and abutment pressure under top coal caving conditions. *International Journal of Rock Mechanics and Mining Sciences*, 2018, 111: 84-93.
- Gocer, F., Sener, N. Spherical fuzzy extension of ahp-aras methods integrated with modified k-means clustering for logistics hub location problem. *Expert Systems*, 2022, 39(2): e12886.
- Guo, D., Xie, H., Gao, M., et al. *In-situ* pressure-preserved coring for deep oil and gas exploration: design scheme for a coring tool and research on the *in-situ* pressure-preserving mechanism. *Energy*, 2024, 286: 129519.
- He, Z., Xie, H., Gao, M., et al. Design and verification of a deep rock corer with retaining the *in situ* temperature. *Advances in Civil Engineering*, 2020, 2020(1): 13.
- Ho, W., Ma, X. The state-of-the-art integrations and applications of the analytic hierarchy process. *European Journal of Operational Research*, 2018, 267(2): 399-414.
- Ilmola, J., Pohjonen, A., Koskenniska, S., et al. Coupled heat transfer and phase transformations of dual-phase steel in coil cooling. *Materials Today Communications*, 2021, 26: 101973.
- Inada, N., Koji, Y. Data report: Hybrid pressure coring system tool review and summary of recovery result from gas-hydrate related coring in the nankai project. *Marine and Petroleum Geology*, 2015, 66: 323-345.
- Ishizaka, A., Labib, A. Review of the main developments in the analytic hierarchy process. *Expert Systems with Applications*, 2011, 38(11): 14336-14345.
- Kazuya, I., Yosuke, K. Bayesian and neural network approaches to estimate deep temperature distribution for assessing a supercritical geothermal system: evaluation using a numerical model. *Natural Resources Research*, 2021, 30(5): 3289-3314.
- Lee, H., Kim, H., Lee, G., et al. Development of pcs and an experiment for performance evaluation. *Journal of the Korean Society of Marine Engineering*, 2015, 39(9): 973-980.
- Li, B., Yuan, J., An, Z., et al. Effect of microstructure and physical parameters of hollow glass microsphere on insulation performance. *Materials Letters*, 2011, 65(12): 1992-1994.
- Li, R., Shan, Z. Study on structure -induced heat transfer capabilities of waterborne polyurethane membranes. *Colloids and Surfaces A-Physicochemical and Engineering Aspects*, 2020, 598: 124879.
- Li, X., Zhang, Y., Ma, Y., et al. Design and experimental study of an improved pressure core sampler for marine gas hydrates. *ACS Omega*, 2024, 9(13): 14977-14984.
- Mahanta, B., Ranjith, P., Vishal, V., et al. Temperature-induced deformational responses and microstructural. *Journal of Petroleum Science and Engineering*, 2020, 192: 107239.
- Mardani, A., Jusoh, A., Zavadskas, E. K. Fuzzy multiple criteria decision-making techniques and applications-two decades review from 1994 to 2014. *Expert Systems with Applications*, 2015, 42(8): 4126-4148.
- Mutambo, V., Kangwa, S., Fisonga, M. Mining method selection for extracting moderately deep ore body using analytical hierarchy process at mindola sub-vertical shaft. *Cogent Engineering*, 2022, 9(1): 2062877.
- Ruckdeschel, P., Philipp, A., Retsch, M. Understanding thermal insulation in porous, particulate materials. *Advanced Functional Materials*, 2017, 27(38): 1702256.
- Saif, T., Lin, Q., Gao, Y., et al. 4D *in situ* synchrotron X-ray tomographic microscopy and laser-based heating study of oil shale pyrolysis. *Applied Energy*, 2019, 235: 1468-1475.
- Sakurovs, R., Day, S., Weir, S., et al. Temperature dependence of sorption of gases by coals and charcoals. *International Journal of Coal Geology*, 2008, 73(3-4): 250-258.
- Sirdesai, N. N., Gupta, T., Singh, T. N., et al. Studying the acoustic emission response of an Indian monumental sandstone under varying temperatures and strains. *Construction and Building Materials*, 2018, 168: 346-361.
- Swanepoel, J., Vosloo, J. C., Van, L. J., et al. Prioritisation of environmental improvement projects in deep-level mine ventilation systems. *Mining, Metallurgy & Exploration*, 2023, 40(2): 599-616.
- Wang, J., Yu, M., Chen, C., et al. Analysis of factors affecting the internal seawater flow performance of pressure-retaining drilling tool for seafloor drill during drilling process. *Geoenergy Science and Engineering*, 2023, 224: 211601.
- Xie, H., Gao, M., Zhang, R., et al. Application prospects of deep *in-situ* condition-preserved coring and testing systems. *Advances in Geo-Energy Research*, 2024, 14(1): 12-24.
- Zhu, H., Liu, Q., Wong, G., et al. A pressure and temperature preservation system for gas-hydrate-bearing sediments sampler. *Petroleum Science and Technology*, 2013, 31(6): 652-662.